J Mater Sci: Mater Electron (2016) 27:6517–6521
DOI 10.1007/s10854-016-4594-2

Facile and reliable synthesis and characterization of bismuth aluminate nanoparticles and its light harvesting applications

S. Akbar Hosseini[1]

Received: 14 December 2015 / Accepted: 26 February 2016 / Published online: 5 March 2016

Abstract Pure bismuth aluminate ($Bi_2Al_4O_9$) nanoparticles were successfully synthesized by a facile and reliable method with the aid of $Bi(NO_3)_3$, $Al(NO_3)_3{\cdot}9H_2O$, and starch without adding external surfactant, capping agent or template. Moreover, starch plays role as capping agent, reducing agent, and natural template in the synthesis $Bi_2Al_4O_9$ nanoparticles. The structural, morphological and optical properties of as obtained products were characterized by techniques such XRD, EDX, VSM, SEM, and UV–Vis. The as-synthesized $Bi_2Al_4O_9$ nanoparticle was utilized as photo-anode material for the fabrication of FTO/TiO_2/$Bi_2Al_4O_9$/Pt-FTO and photocatalyst for degradation of methyl orange to investigation its light harvesting applications.

1 Introduction

Materials at the nanometer scale have been studied for decades because of their unique properties arising from the large fraction of atoms residing on the surface, and also from the finite number of atoms in each crystalline core. Especially, because of the increasing need for high area density storage, the synthesis and characterization of semiconductor nanocrystals have been extensively investigated [1–11]. The sol gel method of preparing oxide powders generally involves polymerization via hydrolysis and condensation of an alkoxide, gelation, and heat treatment under suitable conditions. In recent years $Bi_2M_4O_9$ ($M = Al^{3+}$, Ga^{3+}, Fe^{3+}) compounds with mullite-type structures [12] have obtained considerable technical interest as potential candidates for applications as oxygen-ion conductors or mixed ionic–electronic conductors (MIEC). Common structural items are chains of edge-shared MO_6 octahedra running parallel to the orthorhombic c-axis linked by (M_2O_7) dimers of MO_4 tetrahedra Especially, $Bi_2Al_4O_9$ does not show any phase transition until 1080 °C and has a high chemical stability in hydrogen atmospheres [13, 14], a necessary feature for the application in fuel cells. Tutov and Echerlin described the possibility of orthorhombic bismuth aluminate preparation in 1965 [15–21], as well as defined the synthesis conditions, temperature and melting character of the compound. Among the wet chemical routes, sol–gel technique has been used widely because it has the advantage of producing pure, ultrafine powders at low temperatures, High surface area and pore size distribution [22–28]. In this report, for the first time, we had presented the preparation of $Bi_2Al_4O_9$ nanoparticles by novel sol–gel method at 800 °C in the presence of starch without adding external surfactant, capping agent or template. A green approach for $Bi_2Al_4O_9$ nanoparticles synthesis by utilizing natural template permits the reaction to proceed usually in milder conditions. Although existing chemical approaches have effectively produced well defined $Bi_2Al_4O_9$ nanoparticles, these processes are generally costly and include the employ of toxic chemicals. The synthesized $Bi_2Al_4O_9$ nanoparticles were further used to investigate the photo-anode material for the fabrication of solar cell and photodegradation of methyl orange (MO).

2 Experimental

2.1 Characterization

The magnetic measurement of samples were carried out in a vibrating sample magnetometer (VSM) (Meghnatis

✉ S. Akbar Hosseini
seyedakbarhoseini6@gmail.com

[1] Young Researchers and Elite Club, Science and Research Branch, Islamic Azad University, Tehran, Iran

Daghigh Kavir Co.; Kashan Kavir; Iran) at room temperature in an applied magnetic field sweeping between ±10,000 Oe. X-ray diffraction (XRD) patterns were recorded by a Philips-X'PertPro, X-ray diffractometer using Ni-filtered Cu Kα radiation at scan range of $10 < 2\theta < 80$. The electronic spectra of the bismuth aluminate were obtained on a Scinco UV–Vis scanning spectrometer (Model S-10 4100). The energy dispersive spectrometry (EDS) analysis was studied by XL30, Philips microscope. Scanning electron microscopy (SEM) images were obtained on LEO-1455VP equipped with an energy dispersive X-ray spectroscopy.

2.2 Synthesis of $Bi_2Al_4O_9$ nanoparticles

At first, 1.71 g of $Bi(NO_3)_3$ was dissolved in 50 mL of distilled water. Then, 4.35 of starch was subsequently added to the above solution under magnetic stirring at 70 °C for 30 min. Afterwards, 2.65 g of $Al(NO_3)_3 9H_2O$ was dissolved in 50 mL of distilled water and was added to the above solution under magnetic stirring. A solution was obtained and further heated at 90 °C for 1 h to remove excess water. During continued heating at 110 °C for 1 h, the solution became more and more viscous to become a gel. Finally, the obtained product was calcinated at 800 °C for 2 h in a conventional furnace in air atmosphere and then cooled it to room temperature.

2.3 Photocatalytic experimental

The methyl orange (MO) photodegradation was examined as a model reaction to evaluate the photocatalytic activities of the $Bi_2Al_4O_9$ nanoparticles. The photocatalytic experiments were performed under an irradiation ultraviolet light. The photocatalytic activity of nanocrystalline $Bi_2Al_4O_9$ obtained was studied by the degradation of methyl orange solution as a target pollutant. The photocatalytic degradation was performed with 50 mL solution of methyl orange (0.0005 g) containing 0.1 g of $Bi_2Al_4O_9$. This mixture was aerated for 30 min to reach adsorption equilibrium. Later, the mixture was placed inside the photoreactor in which the vessel was 15 cm away from the ultraviolet source of 400 W mercury lamps. The photocatalytic test was performed at room temperature. Aliquots of the mixture were taken at definite interval of times during the irradiation, and after centrifugation they were analyzed by a UV–Vis spectrometer. The methyl orange (MO) degradation percentage was calculated as:

$$\text{Degradation rate } (\%) = 100\,(A_0 - A_t)/A_0 \quad (1)$$

where A_t and A_0 are the obtained absorbance value of the methyl orange solution at t and 0 min by a UV–Vis spectrometer, respectively.

2.4 Cell fabrication

The $Bi_2Al_4O_9$ paste have been fabricated according to the procedure reported by Gratzel et al. The slurry of $Bi_2Al_4O_9$ prepared via mixing and grinding 1.0 g of $Bi_2Al_4O_9$ powder with ethanol and water in several steps. After that the slurry sonicated to prepare stable mixture of $Bi_2Al_4O_9$ on ethanol and water. The sonicated slurry mixed with binders such as terpineol and ethyl cellulose and sonicated again. Then the ethanol and water removed from slurry with a rotary evaporator and the final paste was prepared [29]. The prepared uniform $Bi_2Al_4O_9$ paste have been coated on fluorinated tin oxide glass (FTO) glass, Pilkington Glass, TEC7) by a doctor blade technique. The active area of electrodes was 0.4 cm^2. After natural drying at room temperature, the electrodes coated with the pastes gradually heated under an air flow at 300 °C for 5 min. The $Bi_2Al_4O_9$ electrodes immersed into ethanolic solution of natural sensitizers and kept at room temperature for 24 h to complete the sensitizer uptake. Electrodes rinsed with ethanol and dried under a nitrogen stream. A Pt coated FTO glass electrode prepared as a counter electrode. The Pt electrode placed over the dye-adsorbed Ag- $Bi_2Al_4O_9$ electrode and the edges of the cell were sealed with 50 mm thick sealing sheet (Surlyn150, Dyesol). Sealing accomplished by pressing the two electrodes together on a double hot-plate at a temperature of about 80 °C. The redox electrolyte consisting of 0.05 M of LiI, 0.05 M of I_2, and 0.5 M of 4-tert-butylpyridine in acetonitrile as a solvent was introduced into the cell through one of the two small holes drilled in the counter electrode. The electrolyte introduced into the cell through one of two small holes drilled in the counter electrode. Finally, these two holes sealed by a small square of sealing sheet.

3 Results and discussion

Crystalline structure and phase purity of as-prepared product has been determined using XRD. The XRD pattern of as-prepared $Bi_2Al_4O_9$ is shown in Fig. 1. Based on the Fig. 1, the diffraction peaks observed can be indexed to pure monoclinic phase of $Bi_2Al_4O_9$ ($a = 7.7190$ A°, $b = 8.1090$ A°, $c = 5.6919$ A°) with space group of Pbam and JCPDS No. 25-1048. No diffraction peaks from other species could be detected, which indicates the obtained sample is pure. From XRD data, the crystallite diameter (Dc) of $Bi_2Al_4O_9$ nanoparticles was calculated to be 37 nm using the Scherer equation:

$$D_c = K\lambda/\beta\cos\theta \text{ Scherer equation}$$

where β is the breadth of the observed diffraction line at its half intensity maximum (400), K is the so-called shape

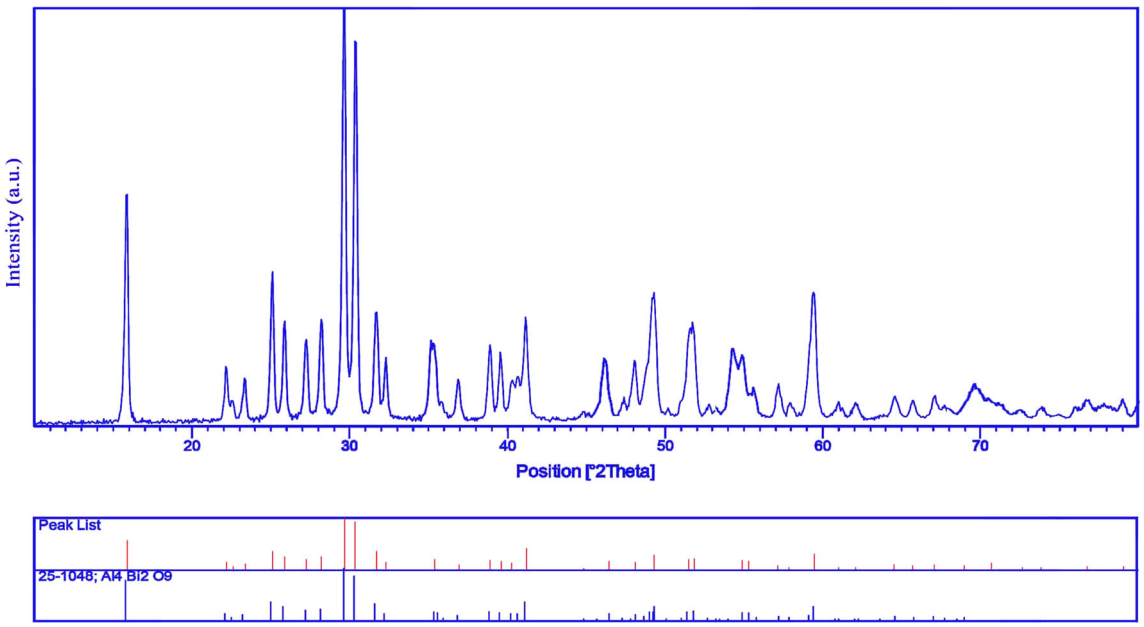

Fig. 1 XRD pattern of $Bi_2Al_4O_9$ nanoparticles calcined at 800 °C

factor, which usually takes a value of about 0.9, and λ is the wavelength of X-ray source used in XRD. The morphology of the nanoparticles was investigated using SEM which demonstrates uniform nanoparticles with spherical shape homogenously distributed all over the sample, as it could be clearly observed in Fig. 2. The $Bi_2Al_4O_9$ nanoparticles with particle size of about 44–50 nm were observed. EDX analysis measurement was employed to investigate the chemical composition and purity of as-synthesized $Bi_2Al_4O_9$ nanoparticles. The EDX pattern of $Bi_2Al_4O_9$ in Fig. 3 exhibits that the only elements which existed were Bi, Al, and O. Furthermore, neither N nor C signals were detected in the EDS spectrum, which means the product is pure and free of any surfactant or impurity. The hysteresis loop of $Bi_2Al_4O_9$ nanoparticles was studied to examine their magnetic properties (Fig. 4). At 300 K the remanent magnetization (Mr) is 0.001 emu/g, the coercive field (Hc) is 85 Oe and the magnetization at saturation (Ms) is estimated to be only 0.007 emu/g (the saturation magnetization Ms was determined from the extrapolation of curve of H/M vs. H). Using Tauc's formula, the band gap can be obtained from the absorption data. The energy gap (Eg) of the $Bi_2Al_4O_9$ nanoparticles has been estimated by extrapolating the linear portion of the plot of $(\alpha h\nu)^2$ against hν to the energy axis. The diffused reflectance spectrum of the as-prepared $Bi_2Al_4O_9$ nanoparticles is shown in Fig. 5. The E_g value is calculated as 3.30 eV for the $Bi_2Al_4O_9$ nanoparticles. Photodegradation of methyl orange as water contaminant under UV light illumination was employed to evaluate the properties of the as-synthesized $Bi_2Al_4O_9$ nanoparticles. Figure 6 exhibits the obtained result. No

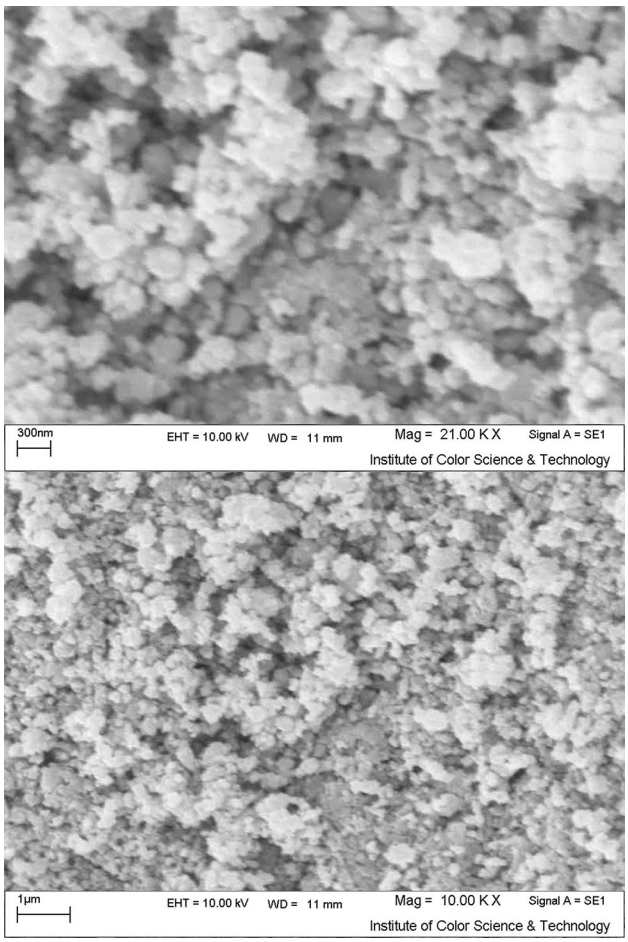

Fig. 2 SEM image of $Bi_2Al_4O_9$ nanoparticles calcined at 800 °C

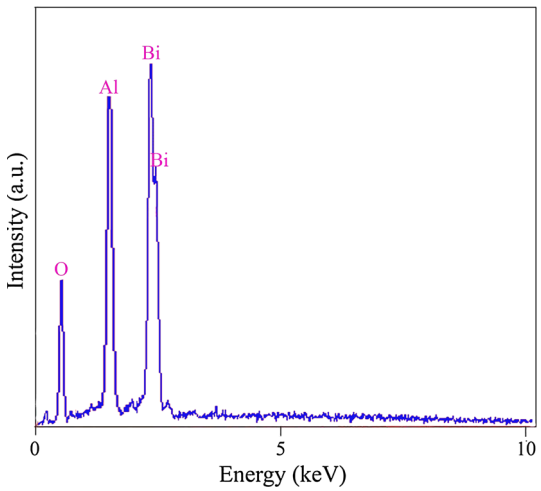

Fig. 3 EDS pattern of $Bi_2Al_4O_9$ nanoparticles calcined at 800 °C

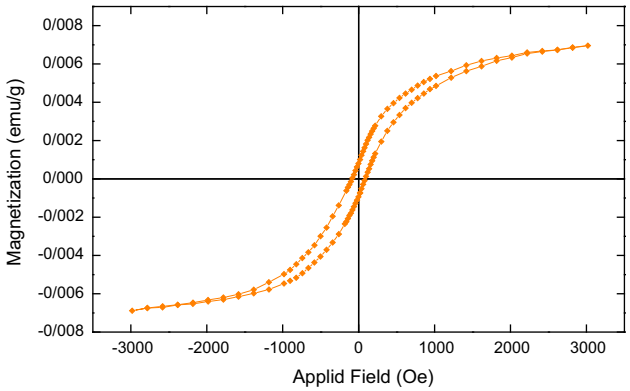

Fig. 4 VSM curve of $Bi_2Al_4O_9$ nanoparticles calcined at 800 °C

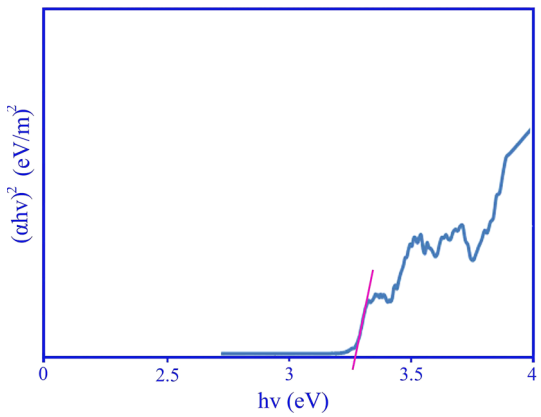

Fig. 5 DRS pattern of $Bi_2Al_4O_9$ nanoparticles calcined at 800 °C

methyl orange was practically broken down after 60 min without employing UV light illumination or as-prepared $Bi_2Al_4O_9$ nanoparticles. This observation illustrated that the contribution of self-degradation was insignificant. The proposed mechanism of the photocatalytic degradation of the methyl orange can be assumed as:

$$Bi_2Al_4O_9 + h\nu \rightarrow Bi_2Al_4O_9^{\cdot} + e^- + h^+ \quad (2)$$

$$h^+ + H_2O \rightarrow OH^{\cdot} \quad (3)$$

$$e^- + O_2 \rightarrow O_2^{\cdot -} \quad (4)$$

$$OH^{\cdot} + O_2^{\cdot -} + \text{methyl orange} \rightarrow \text{Degradation products} \quad (5)$$

Utilizing photocatalytic calculations by Eq. (1), the methyl orange degradation was about 65 % after 60 min illumination of UV light. This obtained result demonstrates that as-prepared $Bi_2Al_4O_9$ nanoparticles have high potential to be applied as favorable and appropriate material for photocatalytic applications under illumination of UV light. The heterogeneous photocatalytic processes have diffusion, adsorption and reaction steps. It has been shown that the desirable distribution of the pore has effective and important impact on the diffusion of the reactants and products, and therefore effects on the photocatalytic activity. It seems that the enhanced photocatalytic activity of the as-obtained nanoparticles $Bi_2Al_4O_9$ can be owing to desirable and appropriate distribution of the pore, high hydroxyl amount and high separation rate of charge carriers (Scheme 1). I–V characterization of a typical solar cell fabricated using in situ approach is shown in Fig. 7 The measurement of the current density voltage (I–V) curve for $Bi_2Al_4O_9$ was carried out under the illumination of AM1.5 (100 mW/cm^2). Device characteristics are as follows: $V_{oc} = 0.4$ V, $J_{sc} = 0.20$ mA/cm^2, FF = 34 %. The V_{oc} and J_{sc} of this device are in order of those obtained using non-vacuum-based techniques. Furthermore, this route is facile to operate and very suitable for industrial production of $Bi_2Al_4O_9$ nanoparticles. In addition, this process can be

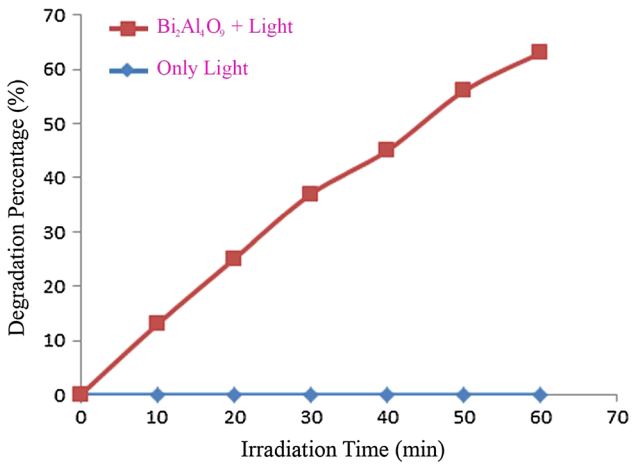

Fig. 6 Photocatalytic methyl orange degradation of $Bi_2Al_4O_9$ nanoparticles under ultraviolet light

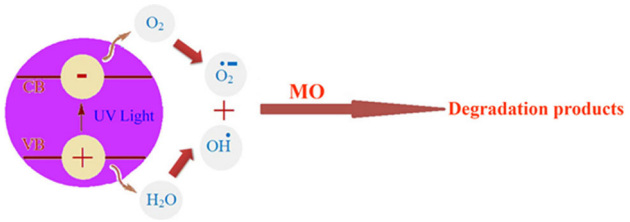

Scheme 1 Reaction mechanism of methyl orange photodegradation over $Bi_2Al_4O_9$ nanoparticles under UV light irradiation

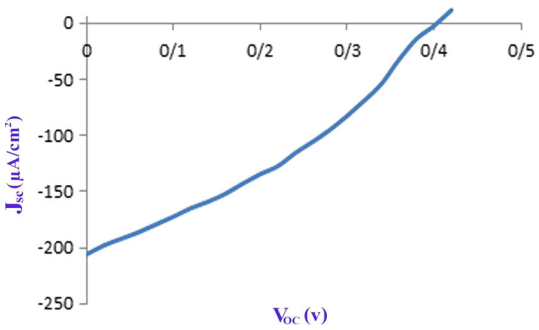

Fig. 7 J–V characterization of $Bi_2Al_4O_9$ nanoparticle calcined at 800 °C

versatile to easily synthesize other aluminate based perovskite oxides.

4 Conclusions

In this work, bismuth aluminate nanoparticles were successfully synthesized by a novel sol–gel method at 800 °C for 120 min. High purity of the as-prepared nanocrystalline sample was proved by XRD, and EDS analyses. When as-prepared nanocrystalline bismuth aluminate was utilized as photocatalyst, the percentage of methyl orange degradation was about 65 % after 60 min irradiation of UV light. This result suggests that as-obtained nanocrystalline bismuth aluminate as favorable material has high potential to be used for photocatalytic applications under UV light. The nature of M–H curve represents ferromagnetic behaviour in $Bi_2Al_4O_9$ nanoparticles. A preliminary study on the possibility of developing a solar cell having FTO/TiO_2/$Bi_2Al_4O_9$/Pt-FTO structure was also performed.

Acknowledgments Authors are grateful to council of University of Science and Research for providing financial support to undertake this work.

References

1. P. Bakhshaei, A. Ataie, H. Abdizadeh, J. NanosStruct. **3**, 403 (2013)
2. R.R. Shahraki, M. Ebrahimi, J. NanosStruct. **2**, 413 (2013)
3. F.S. Ghoreishi, V. Ahmadi, M. Samadpourc, J. NanosStruct. **3**, 453 (2013)
4. S. Moshtaghia, D. Ghanbarib, M. Salavati-Niasari, J. NanosStruct. **5**, 169 (2015)
5. A. Rahdar, M. Aliahmad, Y. Azizi, J. NanosStruct. **5**, 145 (2015)
6. J. Safaei-Ghomi, S. Zahedi, M. Javid, M.A. Ghasemzadeh, J. NanosStruct. **5**, 153 (2015)
7. M. Shakib Nahad, G. Mohammadi Ziarani, A. Badiei, A. Bananc, J. NanosStruct. **3**, 395 (2013)
8. M. Rahimi-Nasarabadi, J. NanosStruct. **4**, 211 (2014)
9. M. Najafi, H. Haratizadeh, M. Ghezellou, J. NanosStruct. **5**, 129 (2015)
10. M. Ahmadzadeh, M. Almasi-Kashia, A. Ramazani, J. NanosStruct. **5**, 97 (2015)
11. V.B.R. Boppana, D.J. Doren, R.F. Lobo, Chemsuschem **3**, 814 (2010)
12. K. Gurunathan, J.O. Baeg, S.M. Lee, E. Subramanian, S.J. Moon, K.J. Kong, Int. J. Hydrogen Energy **33**, 2646 (2008)
13. S.W. Cao, Y.J. Zhu, G.F. Cheng, Y.H. Huang, J. Hazard. Mater. **171**, 431 (2009)
14. T. Debnath, C.H. Rüscher, P. Fielitz, S. Ohmann, G. Borchardt, Ceram. Trans. **217**, 71 (2010)
15. T. Debnath, C.H. Rüscher, ThM Gesing, P. Fielitz, S. Ohmann, G. Borchardt, Ceram. Eng. Sci. Proc. **31**, 81 (2010)
16. J. Maier, B. Bunsenges, Phys. Chem. **90**, 26 (1986)
17. J.S. Piccin, C.S. Gomes, L.A. Feris, M. Gutterres, Chem. Eng. J. **183**, 30 (2012)
18. H. Schneider, in *Mullite*, ed. by H. Schneider, S. Komarneni (Wiley-VCH, Weinheim, 2005), pp. 141–164
19. T.M. Gesing, C.H. Rüscher, J.C. Buhl, Z. Kristallogr. Suppl. **29**, 93 (2009)
20. E.I. Speranskaya, V.M. Skorokov, G.M. Safronov, E.N. Gaidukov, Inorg. Mater. **6**, 1201 (1970)
21. A.G. Tutov, I.E. Myl'nikova, I.N. Parfenov, V.A. Bokov, Phisika Tverdogo Tela. **6**, 1240 (1964)
22. P. Eckerlin, J. Liebertz, Naturwissenschaften **52**, 450 (1965)
23. N. Niizeki, M. Wachi, Z. Krist. **127**, 173 (1968)
24. I. Bloom, M.C. Hash, J.P. Zebrowski, K.M. Myles, M. Krumpelt, Solid State Ion. **739**, 53 (1992)
25. S. Zha, J. Cheng, Y. Liu, X. Liu, G. Meng, Solid State Ion. **156**, 197 (2003)
26. S. Larose, S.A. Akbar, J. Solid State Electrochem. **10**, 488 (2006)
27. ThM Gesing, R.X. Fischer, M. Burianek, M. Mühlberg, T. Debnath, C.H. Rüscher, J. Ottinger, J.C. Buhl, H. Schneider, J. Eur. Ceram. Soc. **31**, 3055 (2011)
28. H.A. Harwig, A.G. Gerards, J. Solid State Chem. **26**, 265 (1978)
29. K. Laurent, G.Y. Wang, S. Tusseau-Nenez, Y. Leprince-Wang, Solid State Ion. **178**, 1735 (2008)